Defects in $Fe_{1-x}O$ and the $Fe_{1-x}O$ to Fe_3O_4 phase transition studied by the perturbed angular correlation method

1991 J. Phys.: Condens. Matter 3 4569

(http://iopscience.iop.org/0953-8984/3/25/006)

J. Phys.: Condens. Matter 3 (1991) 4569–4585. Printed in the UK

Defects in $Fe_{1-x}O$ and the $Fe_{1-x}O \rightarrow Fe_3O_4$ phase transition studied by the perturbed angular correlation method*

Z Inglot, D Wiarda, K P Lieb, T Wenzel and M Uhrmacher

II. Physikalisches Institut, Universität Göttingen, D–3400 Göttingen, Federal Republic of Germany

Received 5 December 1990, in final form 11 March 1991

Abstract. The time differential perturbed angular correlation (PAC) method has been applied to study defects in iron monoxides, using ion-implanted ^{111}In probes. Besides a broad distribution of electric field gradients two well-defined quadrupole coupling constants have been detected: $\nu_Q = 97(4)$ MHz, $\eta = 0$ and $\nu_Q = 71(2)$ MHz, $\eta = 0.32(2)$. The first one was associated with an indium–iron vacancy complex, while the second one, visible in a high-temperature measurement, was tentatively assigned to indium having trapped two iron vacancies and one interstitial iron atom (the so-called Roth-type cluster). Structural transformations between different complexes and the $Fe_{1-x}O \rightarrow Fe_3O_4$ phase transition are discussed. From the analysis of the vacancy/interstitial ratio, a sizeable fraction of 4:1 defect clusters at low temperatures can be excluded. The proposed defects are compared with those recently observed in the chemically and structurally similar cobalt monoxide CoO.

1. Introduction

The ferrous oxide wustite FeO is a material with a defective sodium chloride structure in the paramagnetic phase. Below the Néel temperature ($T_N \approx 200$ K which strongly depends on the deviation from ideal stoichiometry [1]), FeO becomes antiferromagnetic and the structure changes from cubic to rhombohedral with a small distortion along the [111] axis. FeO is thermodynamically unstable below 843 K. Upon quenching as well as upon heat treatment below T_N, Fe_3O_4 nucleates and easily forms islands of different sizes within the wustite structure.

Magnetite (Fe_3O_4) has the cubic inverse spinel structure with half the Fe^{3+} ions on tetrahedral sites (labelled A sites) and the other half on octahedral sites (B sites), whereas all Fe^{2+} ions are located on octahedral sites. Fe_3O_4 is a ferrimagnet with a Néel temperature of 850 K. A Verwey (electronic) transition takes place at $T_V = 120$ K and involves the iron ions on the octahedral sites. Below T_V the octahedral Fe^{3+} ions and Fe^{2+} ions align in mutually perpendicular rows [2]. Above T_V an exchange of a thermally activated d electron of Fe^{2+} takes place between octahedral ions.

Among the four transition metal monoxides with the same structure in the paramagnetic phase (MnO, FeO, CoO and NiO) wustite exhibits the largest deviation from stoichiometry. Using the notation $Fe_{1-x}O$, x extends up to 0.16 [3]. It is generally accepted that the oxygen sublattice is nearly perfect so that $x > 0$ corresponds to

* Supported by Deutsche Forschungsgemeinschaft, Projekt Li325/2-1.

0953-8984/91/254569+17$03.50

the presence of cation vacancies. Charge neutrality requires that some of the iron ions are in the Fe^{3+} state. Neutron diffraction studies [4] revealed that the apparent concentration of vacancies in $Fe_{1-x}O$ exceeds the value of x determined by chemical analysis. This can be explained by assuming that part of the iron ions are located on interstitial tetrahedral sites [5]. Because of the large variety of stoichiometric compositions of $Fe_{1-x}O$, many properties are still unclear and the system is the subject of detailed studies; in particular the nature of defects, their structure, clustering and ordering have been investigated extensively [6–11].

In the past few years, ion implantation of radioactive impurities suitable for perturbed angular correlations (PAC) of γ-rays has become a very powerful tool to study microscopic properties in many metal oxides [12–14]. As examples related to the transition metal monoxides, we refer to recent investigations of supertransferred magnetic fields [15] in NiO, CoO and MnO [16–18] and studies of the $CoO \rightarrow Co_3O_4$ structural phase transition [19]. The main advantage of the PAC technique (compared with macroscopic methods such as x-ray diffraction, neutron scattering or chemical analysis) is the possibility of distinguishing between various microstructures occurring in the nearest neighbourhood of the dilute probe atoms. Thus, the method is able to monitor the changes in the microstructures after subsequent thermal treatments and in this way to supply information about the defect chemistry. Another advantage of the PAC method in comparison with Mössbauer spectroscopy (which is most suitable for investigating iron compounds) is its high and stable sensitivity in a broad temperature range.

The aim of this work was to study the defect structures in $Fe_{1-x}O$ and the $Fe_{1-x}O \rightarrow Fe_3O_4$ phase transition by means of implanted ^{111}In impurity ions. The paper is organized as follows: In section 2 we present a short review of previous experiments as well as the results of theoretical studies related to the subject. In section 3 the PAC method and the experimental procedure are described. The experimental results and their analysis and interpretation are presented in sections 4 and 5.

2. Summary of previous results

Theoretical evidence for the structure of defects comes from lattice energy calculations based on the Born model, performed by Catlow and Fender [10]. These authors examined: (i) simple isolated point defects like cation vacancies, octrahedral Fe^{3+} and tetrahedral Fe^{3+}; (ii) clusters of 1–4 cation vacancies trapped at octahedral Fe^{3+} ions; (iii) defects containing tetrahedral Fe^{3+} ions with up to four Fe vacancies. It was concluded that the $4V_{Fe} + Fe_t^{3+}$ configuration (often called the 4:1 cluster) is the dominating one among the simple defects in $Fe_{1-x}O$. Catlow and Fender [10] also proposed larger stable aggregates of this basic 4:1 defect, i.e. corner-shared clusters (13:4, 16:5), edge-shared clusters (6:2, 8:3, 10:4) and a corner-linked cluster (7:2). Finally, they suggested that nucleation of the inverse spinel structure of Fe_3O_4 occurs via the transformation of 6:2 and 8:3 clusters to 16:5 clusters.

Most experimental studies of $Fe_{1-x}O$ were carried out at high temperature (in the thermodynamical stability region of wustite) or at room temperature (on quenched samples). A cluster configuration consisting of two iron vacancies and one tetrahedral interstitial cation was proposed by Roth [4] as an interpretation of neutron diffraction measurements at room temperature and was later confirmed by the x-ray investigations of Smuts [20]. However, most subsequent experiments favoured larger

defects. The room temperature x-ray studies of Koch and Cohen [7] suggested the existence of clusters with fourteen cation vacancies and four iron interstitials. The room temperature neutron diffraction experiments by Battle and Cheetham [5] and high-temperature neutron diffraction studies by Cheetham *et al* [8] provided support for the existence of 4:1 clusters. More recently, Anderson and Sletnes [6] studied defect ordering in quenched $Fe_{1-x}O$ samples by combining electron diffraction and microscopy. They postulated a cluster size of ten vacancies and three interstitials.

The hyperfine interaction studies of iron monoxides with Mössbauer spectroscopy [21–23] have preferentially explained the experimental findings in terms of simple defects. Shirane *et al* [21] connected the observed quadrupole splitting $\varepsilon = 0.3\ \mathrm{mm\,s^{-1}}$ with cation vacancies which destroy the cubic symmetry at the Fe nucleus. A similar quadrupole splitting was found by Hrynkiewicz and coworkers [22] who investigated samples with x ranging from 0.002 to 0.250. For samples with $x > 0.084$ they observed a double Zeeman splitting which they attributed to the presence of the magnetic phase. Larger defect aggregates were proposed by Greenwood and Howe [11, 24, 25] who performed Mössbauer spectroscopy on quenched $F_{1-x}O$ samples. These authors suggested the formation of clusters of four cation vacancies around a tetrahedral Fe^{3+} ion and the direct transformation of four 4:1 defects towards a 13:4 cluster.

3. PAC method and experimental procedure

3.1. Principle of the PAC method

The theory of perturbed angular correlation (PAC) is well described in several review articles and textbooks, see for example [26]. Here we give only a short introduction to the commonly used formalism and adopted notations. The PAC technique [27] is based on the observation of the γ–γ directional correlation of two γ-rays emitted successively from the PAC probe nucleus [28]. In our case the ^{111}Cd nuclei populated in the EC decay of ^{111}In ($T_{1/2} = 2.7$ d) were the source of the angular correlated 171–245 keV gamma cascade with the intermediate isomeric state (mean life $\tau = 122$ ns, spin $I = 5/2^+$, quadrupole moment $Q = 0.83$ b, magnetic moment $\mu = -0.766\ \mu_N$) probing the local magnetic field and/or the electric field gradient (EFG). As usual, the experimental perturbation function $R(t)$

$$R(t) = 2\frac{N(t,\Theta = 180°) - N(t,\Theta = 90°)}{N(t,\Theta = 180°) + 2N(t,\Theta = 90°)} \tag{1}$$

was extracted from the time differential coincidence rates $N(t,\Theta = 180°)$ and $N(t,\Theta = 90°)$. This ratio is directly related to the perturbation factor $G_2(t)$

$$R(t) = A_{22}^{\mathrm{eff}} G_2(t). \tag{2}$$

The effective anisotropy coefficient A_{22}^{eff} of the γ–γ cascade depends on the spins of the nuclear states, the multipolarities of the gamma radiations and the detector geometry [29]. The perturbation factor $G_2(t)$ contains all the information on the hyperfine interactions between the quadrupole moment Q of the probe nucleus in its intermediate state and the electric field gradient, and/or the nuclear magnetic moment μ and the local magnetic field H_{hf}. As the results presented in the following sections will be described in terms of either the pure magnetic dipole interaction or electric quadrupole

interaction, we do not discuss the case of combined electric and magnetic hyperfine interaction. Often the total observed disturbance of the angular correlation results from different hyperfine interactions. The experimental perturbation function is then expressed as

$$R(t) = A_{22}^{\text{eff}} \sum_{i=1}^{m} f_i G_2^i(t) \qquad \left(\sum_i^m f_i = 1 \right) \tag{3}$$

where f_i represents the fraction of probe atoms with the same local environment and thus being exposed to the same EFG or magnetic field.

The EFG tensor is completely defined by two independent parameters: the component with the largest magnitude $V_{zz}(|V_{zz}| \geq |V_{yy}| \geq |V_{xx}|)$ and the asymmetry parameter $\eta = (V_{xx} - V_{yy})/V_{zz}$. For a polycrystalline sample exhibiting randomly oriented EFG the perturbation factor is usually parametrized as in [26]:

$$G_2(t) = \sum_{n=0}^{3} s_{2n}(\eta) d(g_n(\eta)\nu_Q; \tau_r) \cos[g_n(\eta)\nu_Q t] \exp[-g_n(\eta)\delta t]. \tag{4}$$

The factor $d(g_n(\eta)\nu_Q; \tau_r)$ takes into account the finite time resolution τ_r of the apparatus [30]. The EFG is characterized by the quadrupole coupling constant $\nu_Q = eQV_{zz}/h$, the asymmetry parameter η and the width of the Lorentzian distribution δ around ν_Q. The coefficients s_{2n} of the harmonics can be calculated by diagonalizing the Hamiltonian for the hyperfine interaction of the EFG with the nuclear quadrupole moment [26]. Finally, the functions $g_n(\eta)$ give the relation between the transition frequencies $\omega_n (n = 1\text{–}3)$ in the quadrupole splitted intermediate state and the quadrupole coupling constant ν_Q via the relationship $\omega_n = g_n(\eta)\nu_Q$.

In the case of a magnetic dipole interaction randomly oriented in space, the $R(t)$ function is analysed with the expression

$$G_2(t) = \sum_{n=0}^{2} s_n \cos(n\omega_L t) \exp(-n\delta_L t) \tag{5}$$

where H_{hf} is related to the Larmor frequency $\omega_L = \mu_N g H_{hf}/h$.

3.2. Experimental details

In this section we specify the sample preparation and heat treatments and give some details of the PAC measurements. Commercially available powders of FeO and Fe_3O_4 (Johnson-Matthey; purity 99.99%) were pressed onto silver foils. The FeO structure was verified via x-ray diffraction. The Göttingen heavy ion implanter IONAS [31] enabled us to introduce the ^{111}In activity via ion implantation. A total dose of some 10^{12} $^{111}In^+$ ions was implanted with an energy of 400 keV. The maximum concentration of ^{111}In in the implantation profile was less than 10^{-2} at.%.

The following sets of PAC measurements were carried out where the indexes a and m refer to annealing and measuring conditions:

(1) PAC spectra were taken at room temperature after subsequent *isochronal* annealings of $Fe_{1-x}O$ at the temperature $T_a = 300\text{–}773$ K, the annealing time $t_a = 30$ min and the oxygen pressure $p_a(O_2) < 0.16$ mPa.

(2) The second set of PAC spectra in $Fe_{1-x}O$ was taken at room temperature after successive *isothermal* annealings of $Fe_{1-x}O$ samples at $T_a = 373$ K and with t_a ranging between 30 and 240 min. The partial oxygen pressure was below 0.16 mPa. A final 24-h PAC measurement was recorded at $T_m = 373$ K and $p_m(O_2) < 0.2$ mPa.

(3) After implantation into $Fe_{1-x}O$ two successive measurements at $T_m = 373$ K and 873 K were taken, $p_m(O_2)$ being less than 0.2 mPa in both cases. Another high-temperature measurement was performed at 893 K. A low-temperature measurement at $T_m = 14$ K was carried out for a ^{111}In-doped sample which had been annealed at 373 K.

(4) Finally, a ^{111}In-implanted Fe_3O_4 sample was annealed at 773 K ($t_a = 30$ min, $p_a(O_2) < 0.16$ mPa) and PAC data were taken at room temperature, 373 and 873 K, all at $p_m(O_2) < 0.2$ mPa.

As usual for each set of measurements, an as-implanted PAC spectrum was taken. The PAC measurements were performed with a conventional slow–fast four detector apparatus equipped with NaI(Tl) detectors, with each detector registering start and stop events. Some measurements were done by means of a fast–fast arrangement with BaF_2 detectors. More details are available in [32]. All $R(t)$ spectra were fitted using the program MINUIT [33].

4. Results

4.1. ^{111}In implanted into Fe_3O_4

We start the presentation of the experimental results with the PAC measurements in the magnetite Fe_3O_4. We have chosen these $R(t)$ spectra in order to be able to monitor the presence of Fe_3O_4 within the $Fe_{1-x}O$ structure. Detailed PAC studies of this system are in progress and will be published later.

Several $R(t)$ functions as well as their Fourier transforms are displayed in figure 1. The first spectrum from the top relates to the measurement at room temperature after annealing at 773 K. The perturbation function exhibits two well defined Larmor frequencies $\omega_{L1} = 173(1)$ MHz and $2\omega_{L1}$ and shows two additional broad frequency distributions around $\omega_{L2} = 164(5)$ MHz and $2\omega_{L2}$. The observation of these two frequency doublets suggests pure magnetic hyperfine interaction and the data were fitted with equation (5). These two fractions are also sufficient to describe the $R(t)$ function taken at 373 K (see figure 1(*b*)), but significant changes of the Larmor frequencies were observed: ω_{L1} (373 K) = 159(1) MHz and ω_{L2} (373 K) = 151(3) MHz. Both spectra are characterized by the same ratio of fractions $f(\omega_{L1})/f(\omega_{L2}) = 4.1(3)$. Finally, the $R(t)$ function measured at 873 K is typical for electric quadrupole interaction: most of the ^{111}Cd nuclei (77%) do not experience any EFG ($\nu_{Q1} = 0$). The remaining probe nuclei, with nearly equal fractions f_2 and f_3, are subject either to an axially symmetric EFG with $\nu_{Q2} = 42(2)$ MHz and $\delta_2 = 3$ MHz and to an asymmetric EFG represented by $\nu_{Q3} = 136(4)$ MHz, $\delta_3 = 26$ MHz and $\eta_3 = 0.59$, respectively. All hyperfine parameters are listed in table 1.

4.2. Isochronal annealing of $Fe_{1-x}O$

Examples of the perturbation functions taken in the isochronal annealing course of $Fe_{1-x}O$ are depicted in figure 3. The hyperfine parameters which describe the $R(t)$ functions of this programme are also listed in table 1. The variations of the fractions

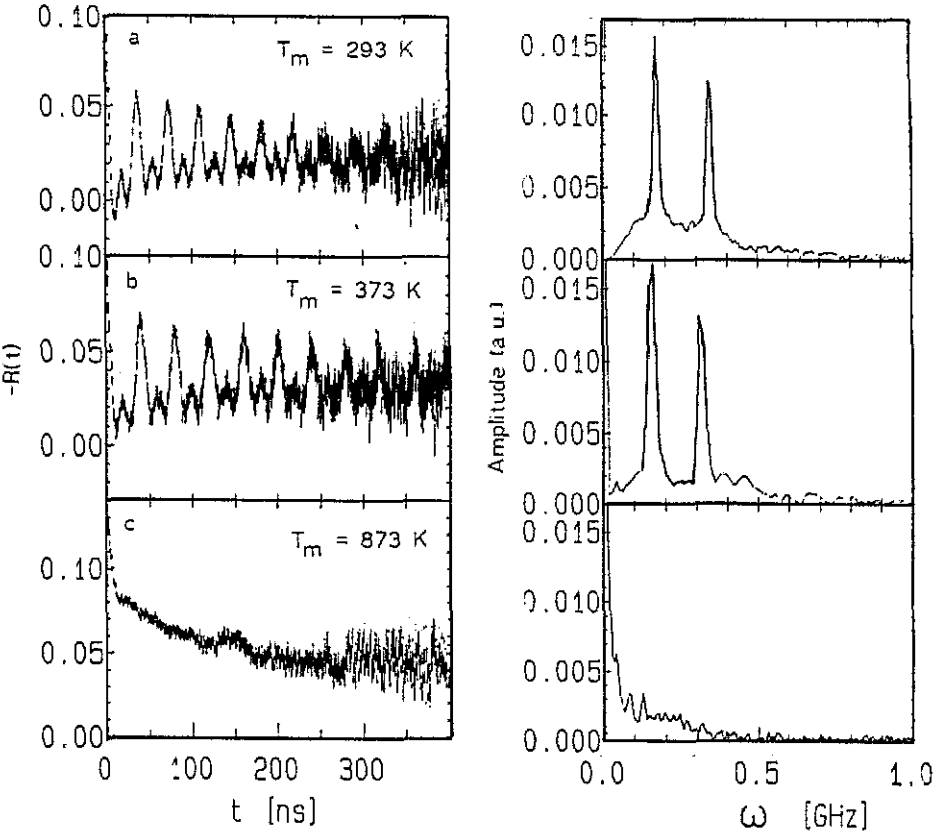

Figure 1. The $R(t)$ functions and their Fourier transforms of ^{111}Cd in Fe_3O_4 measured below the Néel temperature T_N (a) and (b) as well as above T_N (c).

f_i representing different surroundings of ^{111}In after subsequent annealings are shown in figure 4. The as-implanted sample (figure 3(a)) is characterized by two fractions with broadly distributed quadrupole frequencies: f_4 refers to an axially symmetric complex with ν_{Q4} = 97(3) MHz and δ_4 = 38(5) MHz. While the parameter ν_{Q4} was quite stable in all as-implanted spectra, the other parameters varied within the following ranges: δ_4 (25–38 MHz), ν_{Q5} (40–61 MHz) and δ_5 (30–50 MHz). It was possible to improve some fits by introducing another small fraction $f_6 \leq 5\%$ with $\nu_{Q6} = 0$ MHz, $\delta_6 < 6$ MHz and $\eta_6 = 0$.

After the first annealing at 373 K some changes were observed: a small increase in f_4 accompanied by the reduction in δ_4 to 17(2) MHz, a significant decrease in f_5 and the appearance (or increase) of f_6. Next, considerable changes took place after the annealiing at 523 K, where f_6 dropped to zero, f_5 started to decrease and simultaneously the Larmor frequency ω_{L1} = 172 MHz known from Fe_3O_4 appeared. After the 673 K annealing all three fractions f_4, f_5 and f_1 reached more or less stable values. Starting from the annealing at 523 K, a rise in δ_4 was noticed up to 30 MHz at 773 K, while δ_1 decreased from 19(3) to 7(1) MHz.

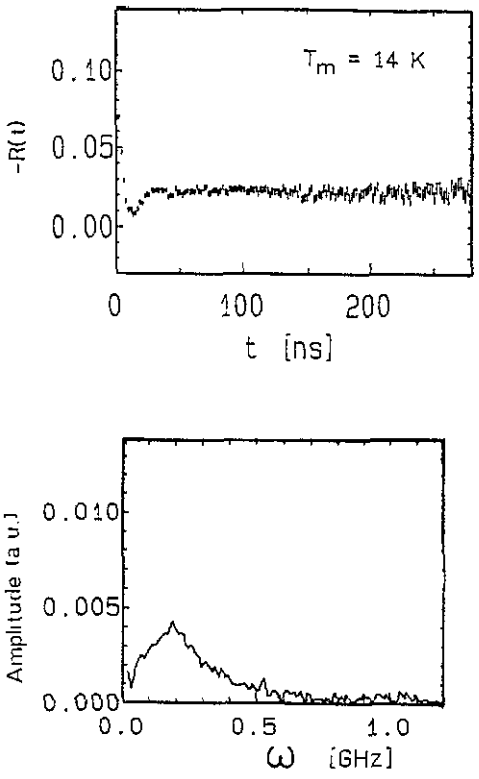

Figure 2. The $R(t)$ function and its Fourier transform of ^{111}Cd in $Fe_{1-x}O$ measured below the Néel temperature.

4.3. Isothermal annealing of $Fe_{1-x}O$

The three fractions f_4–f_6 introduced in the previous section were sufficient to describe all $R(t)$ functions obtained in the course of the isothermal annealing at 373 K. Their small changes after successive annealings are shown in figure 5. All hyperfine interaction parameters were also found to be quite stable. The separated points in figure 5 (not connected with the other ones) represent the measurement performed at 373 K. With the exception of reduced δ_4 and δ_5 values, all other EFG parameters were the same as in the room temperature measurement.

4.4. High-temperature PAC measurements in $Fe_{1-x}O$

The results of the PAC measurements at different measuring temperatures are shown in figure 6. The perturbation function measured at 873 K (figure 6(*b*)) where $Fe_{1-x}O$ is thermodynamically stable, compared with the one measured at T_m = 373 K (figure 6(*a*)), contains a second well-defined quadrupole interaction with ν_{Q7} = 71(2) MHz, δ_7 = 6.5(5) MHz and η_7 = 0.32(2). It is clearly visible in figure 7 that the production of this fraction f_7 is associated with a decrease in fractions f_{4-6}. No significant differences were detected in the fractions when the high-temperature measurement was performed either directly after implantation or after the 373 K measurement.

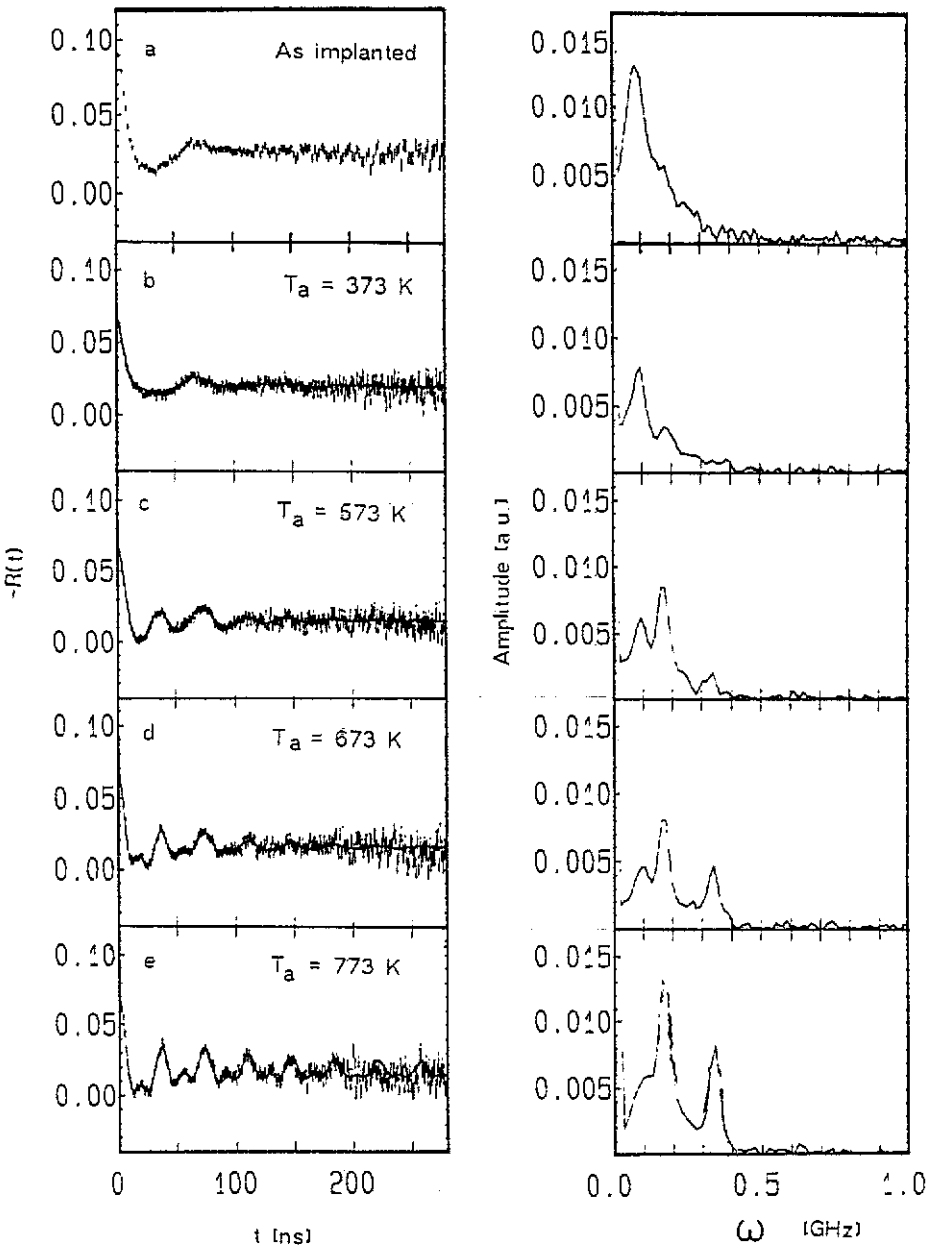

Figure 3. Perturbation functions and associated Fourier transforms representing characteristic stages after subsequent isochronal annealings of $Fe_{1-x}O$. The first spectrum shows the as-implanted state of the sample.

5. Interpretation

5.1. Fe_3O_4

As the implanted In ions are expected to replace, at least partially, Fe ions, we will try to correlate the observed magnetic hyperfine doublets in Fe_3O_4 with the population of

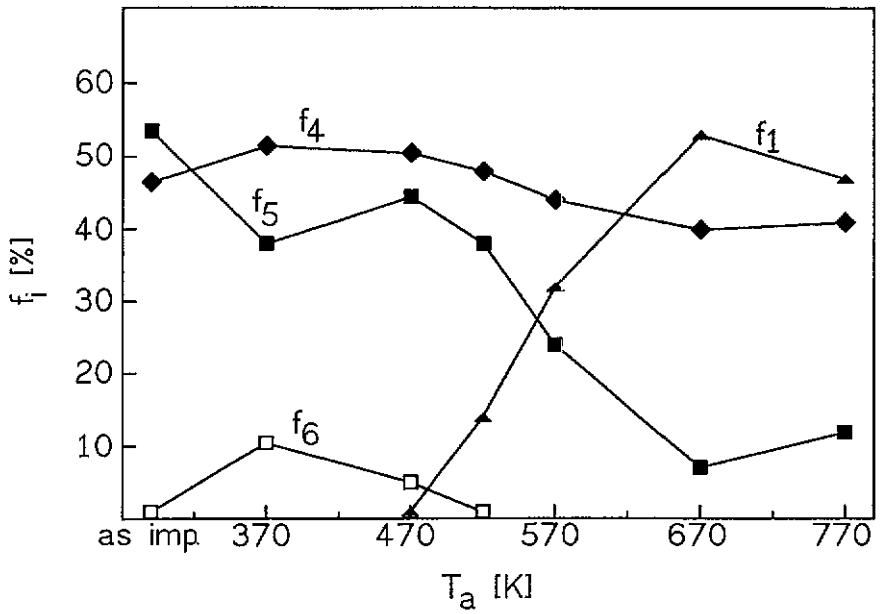

Figure 4. Variation of the fractions f_1, f_4–f_6 in the PAC spectra of the isochronal annealing programme of $Fe_{1-x}O$.

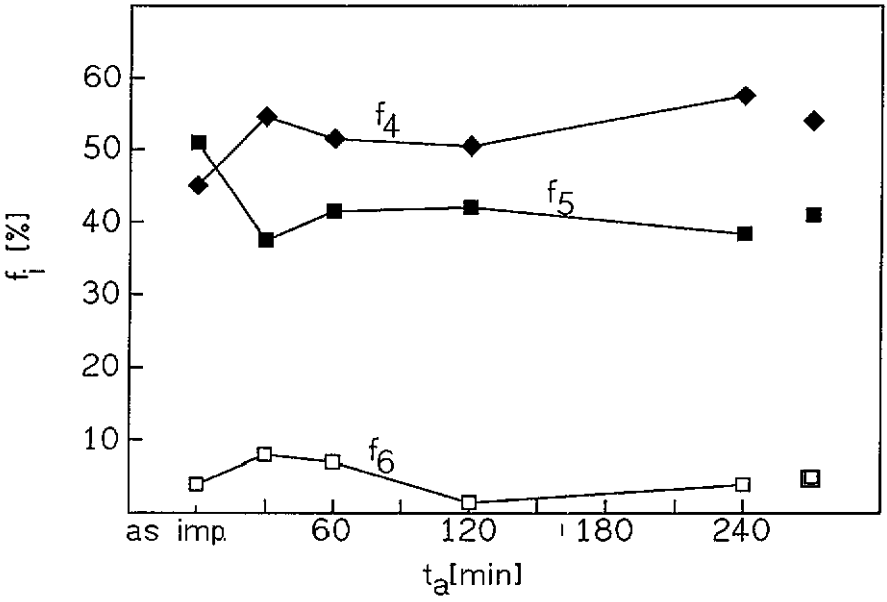

Figure 5. Fractions f_4–f_6 of ^{111}Cd in complexes after isothermal annealings at T_a = 373 K. The points to the right come from the measurement at T_m = 373 K.

the A and B site positions in the inverse spinel structure. Using the value of −0.306 for the nuclear g-factor in ^{111}Cd [34], we obtain from the measured Larmor frequency ω_{L1}(RT) = 173(1) MHz the hyperfine field H_1 = 11.8(1) T at room temperature. This number is in very good agreement with the result H_1 = 12.1 T reported by

Table 1. Hyperfine interaction parameters of ^{111}Cd in Fe_3O_4 and $Fe_{1-x}O$.

(a) Magnetic interactions in Fe_3O_4				
T (K)	ω_{L1} (MHz)	δ_{L1} (MHz)	ω_{L2} (MHz)	δ_{L2} (MHz)
293	173(1)	2.5(5)	164(5)	28(3)
373	159(1)	2.0(5)	151(3)	24(5)

(b) Electric quadrupole interactions in Fe_3O_4			
Fraction	ν_Q (MHz)	δ (MHz)	η
f_1	0	<4	0
f_2	42(2)	3	0
f_3	136(4)	26	0.59(4)

(c) Electric quadrupole interactions in $Fe_{1-x}O$			
	ν_Q (MHz)	δ (MHz)	η
f_4	97(3)	11(1)[a]	0
f_5	34–61	22[a]–50	0.5–0.9
f_6	0	<6	0
f_7[b]	71(2)	6.5(5)	0.32(2)

[a] The lowest value of δ refers to the measurement at 373 K.
[b] Measured at 873 K.

Asai *et al* [35]. These authors performed a PAC experiment on ^{111}Cd/^{111}In probes in Fe_3O_4 in the temperature range of 85–300 K, with an external magnetic field applied perpendicularly to the detector plane. They attributed the hyperfine field of 12.1 T to ^{111}Cd at the tetrahedral position (A site).

This interpretation of ω_{L1} is further corroborated by Mössbauer experiments in Fe_3O_4 [36]. The room-temperature Mössbauer spectra consist of two well-resolved Zeeman patterns with intensities in the ratio 1:2. The deduced hyperfine fields are in the ratio $H^A/H^B = 1.07$ and the B-site linewidth was observed to be considerably larger than the A-site linewidth. This difference in linewidths is still not fully understood [37]. A direct comparison of our results ($\omega_{L1}/\omega_{L2} = 1.05$ and a similar difference in linewidths δ_{L1} and δ_{L2}) with those from Mössbauer spectroscopy suggests the second PAC Larmor frequency ω_{L2} should be interpreted as being due to ^{111}Cd atoms at the B site. However, one should be cautious with this assignment, as the observed broad frequency distribution around ω_{L2} might also arise from a superposition of several distinct patterns. A more definite interpretation may be gained from further detailed studies of this system, in particular using a single crystal. It is evident that the decrease in both Larmor frequencies at the higher measuring temperature $T_m = 373$ K is due to the thermal excitation of the atomic spins and staggered magnetization, as expected from a Curie–Weiss-type critical behaviour.

Now we would like to discuss the results of the PAC measurement taken at 873 K, i.e. above the Néel temperature. We first note that the fraction f_1 with the well-defined Larmor frequency ω_{L1} has disappeared; instead, 77% of the ^{111}Cd probes feel no hyperfine interaction at all. Indeed, the cubic symmetry of the A site implies vanishing EFG at the probe atom in this position. The origin of the two fractions f_2 and f_3 with finite EFGs detected at this high temperature is less clear. The axially

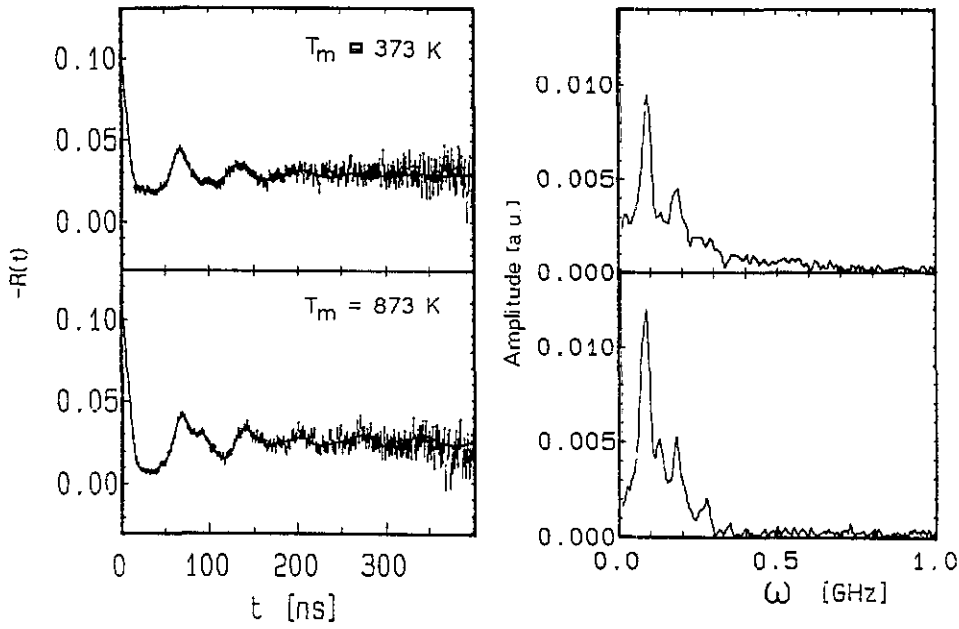

Figure 6. PAC spectra and Fourier transforms for ^{111}Cd in $Fe_{1-x}O$ measured at 373 and 873 K.

symmetric EFG (f_2) could be related to the defect-free octahedral B position, while the other one (f_3) could be connected with a deformed octahedron or simple point defects such as cation vacancies or interstitials. These point defects have been proposed to explain the high-temperature diffusion data in magnetite [9].

5.2. $Fe_{1-x}O$

5.2.1. Antiferromagnetism. In many transition-metal monoxides nearly 100% of the implanted ^{111}In ions enter substitutional metal sites. This was the case in NiO, CuO and CoO as was confirmed by studies of the supertransferred magnetic field and its temperature dependence [12, 16, 17]. Unfortunately, we have not observed any well-defined signal in the low-temperature (T_m = 14 K) PAC measurement of an annealed $Fe_{1-x}O$ sample which could be attributed to pure magnetic hyperfine interaction. The supertransferred magnetic field and the Néel transformation of impurity atoms in wustite, indeed, may be very difficult to observe by the PAC method: the antiferromagnetism could be strongly masked by (i) the presence of different defects which could create paramagnetic and ferromagnetic islands within the bulk material [4, 38]; and (ii) in the case of probe nuclei with a large quadrupole moment, by strong EFGs which would cause the Fourier spectrum to split into many components. In the low-temperature measurement only a very broad frequency distribution was detected (see figure 2) which is different from that visible in the room temperature experiment and possibly represents several types of magnetically ordered defects. An additional explanation comes form a direct comparison of as-implanted $Fe_{1-x}O$ and $Co_{1-x}O$ samples at $T > T_N$ [19, 39]. The $R(t)$ function of ^{111}Cd in $Co_{1-x}O$ is characterized by an 80% fraction with $\nu_Q = 0$ representing ^{111}In at defect-free cation sites, while the former one exhibits not more than 5% of such a cubic fraction. This dramatic

difference between the two monoxides is probably due to their natural deviation from stoichiometry: for $x < 0.01$ in $Co_{1-x}O$ the chance of finding a nearest-neighbour vacancy at the In site is smaller than in $Fe_{1-x}O$.

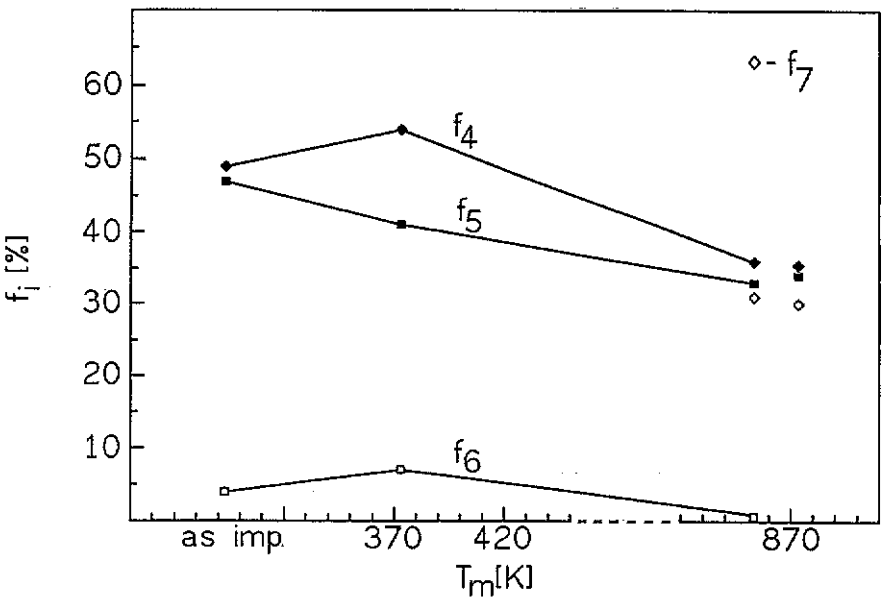

Figure 7. Evolution of fractions f_{4-6} and appearance of fraction f_7. After the measurement at $T_m = 373$ K, the sample was heated to the temperature where $Fe_{1-x}O$ is thermodynamically stable. The measurement at 873 K was recorded without any previous thermal treatment.

5.2.2. Defect configurations. The authors of the previous x-ray and neutron diffraction and hyperfine interaction experiments (see section 2) have mainly concentrated on one type of defect under specific thermodynamic conditions. The interpretation of the present results requires the assumption that several types of defects coexist.

(1) f_4. We tentatively attribute this fraction, which rises up to 52%, to ^{111}In atoms on substitutional Fe sites with one nearest-neighbour vacancy in the metallic sublattice. This interpretation is based on the following considerations: f_4 has been observed after implantation where the distribution of radiation-induced vacancies overlaps with the ^{111}In implantation profile. Axially symmetric EFGs attributed to monovacancies have also been observed in Mössbauer spectroscopy (MS) experiments [21–23]. Indeed, the point charge model (PCM) predicts axial symmetry for this complex (see later). Finally, the similarity of the coupling constants measured for ^{111}Cd in $Fe_{1-x}O$ and the structurally and chemically similar CoO [19] corroborates this conjecture (see table 3). The postulated In–V_{Fe} complex is more visible in the isothermal PAC spectra at 373 K where it has a small width parameter $\delta_4 = 11$ MHz (see figure 6), compared with the strong damping of this fraction at room temperature ($\delta_4 \approx 30$ MHz). This decrease in δ_4 for increasing temperature may be correlated with so-called after-effects observed in many semiconducting and insulating oxides. These effects are a consequence of the electron capture (EC) decay of the ^{111}In nucleus and the large time constants required

to re-establish an unperturbed electron configuration in the ^{111}Cd daughter atom [28]. A recent PAC survey of ^{111}Cd implantations in many metal oxides has revealed that, indeed, the room temperature damping is mainly due to the ^{111}In decay [40].

(2) f_5 and f_6. f_5 is characterized by a very broad frequency distribution. In the isothermal programme, it partially emerges after the first 30 min annealing. In the isochronal annealing cycle, fraction f_5 transforms into the magnetic fraction typical for the Fe_3O_4 phase (see figure 4). Due to the broadly distributed EFG, we cannot give a unique interpretation of this fraction, but suggest that it contains several clusters of different size consisting of iron vacancies and interstitials.

We have also found evidence for a small fraction f_6 with vanishing EFG which we attribute to substitutional impurity atoms on unperturbed sites. This fraction emerges after the first 373 K annealing and has disappeared above 500 K. We tentatively associate the f_5 and f_6 with the segregation of $Fe_{1-x}O$ into vacancy-poor and vacancy-rich phases [11, 41] which are connected with the migration and agglomeration of existing vacancies in the first steps of the $Fe_{1-x}O \rightarrow Fe_3O_4$ phase transformation. It is plausible to assume that the cubic f_6 is located in the vacancy-poor region of $Fe_{1-x}O$, while the highly disturbed f_5 may be located in the vacancy-rich region.

In order to test our proposed association of f_{4-6} with the $Fe_{1-x}O$ phase, we carried out an x-ray diffraction analysis of the sample after the 373 K isothermal annealing. Since no Bragg reflexes due to Fe_3O_4 nor additional ones could be observed, we conclude that the sample still is in the iron monoxide phase.

(3) f_7. This is the second fraction with well-defined quadrupole interaction parameters. Figure 7 suggests that this fraction ($f_7 \approx 30\%$ at 853 K) mainly originates from the decrease in f_4 by 20% between 373 and 853 K. Its interpretation as an interstitial Fe^{3+} ion decorated with two Fe vacancies (Roth-type cluster [4]) is based on PCM arguments presented later.

5.2.3. EFG estimates with the PCM. The PCM has been adopted as a guide in distinguishing between different complex configurations and in describing transformations between them. These calculations require information about the polarizability of conduction electrons and the probe atom shell. While one can neglect the former contribution in semiconductors, the second one enhances the EFG by at least an order of magnitude, relative to PCM. Another limitation of the PCM is related to the lattice relaxation in the neighbourhood of the probe atom. The calculated EFG is, indeed, very sensitive to small changes in the atomic coordinates. In spite of these well known shortcomings, the PCM often provides reasonable estimates for the asymmetry parameter η and the ratio of quadrupole frequencies. As an example, we mention the results of our PAC experiments on ^{111}Cd in CoO (see table 2) where the defect configurations had also been attributed on the basis of the PCM [19]. Indeed the predicted vanishing asymmetry parameters and the 2:1 frequency ratio of the linear V_{Co}–In_s–V_{Co} and In_S–V_{Co} complexes nicely agreed with the measurement.

Several complexes have been examined and the calculated EFG parameters are presented in table 3. These calculations were performed by including all atoms in a shell of 50 Å radius around the probe atom. The frequencies were normalized with respect to that of the presumed In-monovacancy configuration (ν_{Q4}). When comparing the calculated asymmetry parameters η and frequency ratios, it appears that the parameters of f_7 best fit to a $2V_{Fe}$–In_s–Fe^{3+} cluster where the interstitial Fe^{3+} ion is coordinated by an oxygen tetrahedron (so called Roth-type cluster).

Table 2. Experimental PAC parameters for defects in transition metal monoxides trapped to ^{111}In.

	ν_Q (MHz)	η	Interpretation
$Co_{1-x}O$ [19]	81(2)	0	In_s–V_{Co}
	163(1)	0	V_{Co}–In_s–V_{Co} [a]
$Fe_{1-x}O$	97(3)	0	In_s–V_{Fe}
	71(2)	0.32(2)	$2V_{Fe}$–In_s–Fe_t^{3+} [b]

[a] Linear molecule.
[b] Roth-type cluster.

Table 3. Results of the PCM calculations for selected defect configurations in iron monoxide.

	Exp.	V_{Fe}–Fe_s^{3+}	$2V_{Fe}$–Fe_t^{2+}	$2V_{Fe}$–Fe_t^{3+}
(ν_Q/ν_{Q4})	0.73(3)	1.76	0.74	0.64
η	0.32(2)	0.72	0.84	0.32

Fe_s: Fe ion at its normal substitutional position.
Fe_t: Fe ion at interstitial position coordinated by anion tetrahedron.

We now shortly discuss the charge transfer associated with the transformation of f_4 into f_7. Figure 8 depicts the proposed atomic configurations as previously discussed: the nearest-neighbour substitutional Fe^{2+} ion jumps into the interstitial Fe^{3+} position thereby releasing one electron. This explanation is in line with the temperature-dependent change from p- to n-type conductivity in the iron monoxide [23]. Localization of the sixth d-electron at the interstitial Fe ion, i.e. formation of the $2V_{Fe}$–Fe_t^{2+} complex, seems to be less likely, on the basis of the asymmetry parameter predicted by the PCM (see table 2).

It is possible that the interstitial iron ion is involved in an electron hopping process. Such electron hopping has been found in Fe_3O_4 [36] and has been postulated to occur in $Fe_{1-x}O$ in the presence of large defect aggregates [25]. We do not know the electron hopping frequency in $Fe_{1-x}O$. If we assume that this frequency is not much smaller than that predicted for Fe_3O_4 ($\nu^{-1} = 1.1(2)$ ns at room temperature [36]), an electronic state with an average charge of +2.5 should be taken for the interstitial and one of the nearest-neighbour iron ion. PCM estimates for this configuration gave $\eta = 0.5$ and $\nu_Q/\nu_{Q4} \approx 0.7$.

5.2.4. Vacancy–interstitial ratio. In $Fe_{1-x}O$, the iron vacancy/iron interstitial ratio (V/I) provides a guide to the cluster size [5–8]. For the various defect clusters proposed in the analysis of neutron, x-ray and electron diffraction and microscopy experiments presented in section 2, V/I varies from 2.8 to 4.2. Based on the fractions f_1 found in the PAC measurements and their proposed defect configurations, we can estimate V/I and compare these values with the previous results. In our calculation we have assumed that the fractions f_6, f_4 and f_7 represent probe atoms having in their nearest surroundings no defect, one vacancy and two vacancies + one interstitial. Furthermore, we assume, at this stage, that the fraction f_5 also has a well-defined vacancy/interstitial ratio for which we adopted the values postulated in the literature, i.e. 4:1, 6:2, 7:2, 8:3, 10:3, 10:4, 13:4 and 16:5. The calculated V/I ratios are plotted in figure 9 in comparison with the values from [5–8]. The overall agreement is

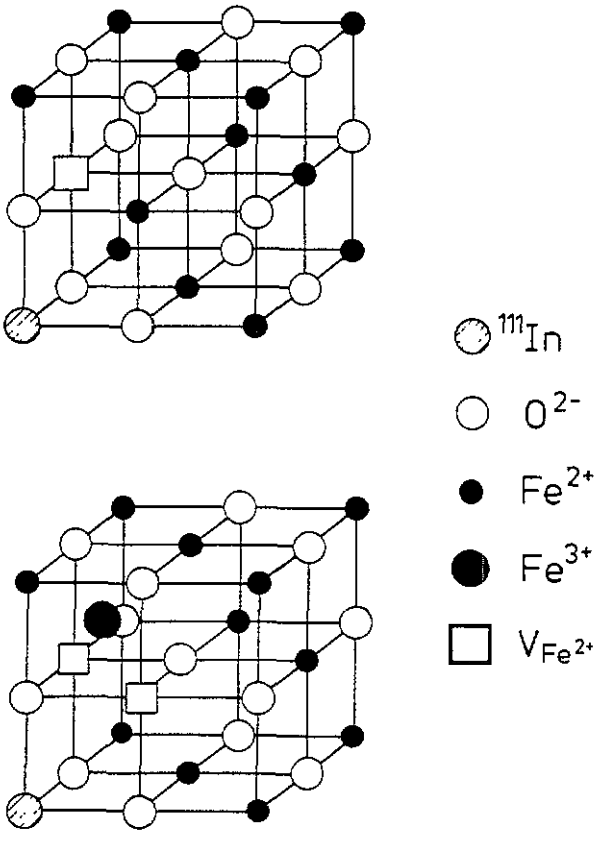

Figure 8. The proposed structural transformation between In–V_{Fe} and In_s–($2V_{Fe}$–Fe_t^{3+}) complexes.

surprisingly good. Although we cannot differentiate between the various defect clusters with $V/I \leq 4$, the results show that the formation of the 4:1 cluster is not the predominant process at 373 K (curve a).

6. Conclusions

The PAC method with $^{111}In/^{111}Cd$ probes has been employed to study the $Fe_{1-x}O \rightarrow Fe_3O_4$ phase transition and the defect structures in $Fe_{1-x}O$. We have demonstrated that this method is well suited to distinguish between different local environments of the nuclear probe. A well-defined hyperfine field has been measured in the ferrimagnetic Fe_3O_4 corresponding to the Larmor frequency $\omega_{L1} = 173(1)$ MHz at room temperature. It has been associated with the presence of ^{111}Cd on substitutional A sites in the inverse spinel structure of magnetite. The same signal has been observed in the isochronal annealing process of $Fe_{1-x}O$ above 500 K.

Guided by the PCM and its success in the structurally and chemically similar CoO, we assigned various measured electric field gradients in $Fe_{1-x}O$ to specific defect structures: the quadrupole coupling constants $\nu_{Q4} = 97(3)$ MHz, $\eta_4 = 0$ were identified with In_s–V_{Fe} pairs, while the quadrupole interaction parameters $\nu_{Q7} = 71(2)$ MHz, $\eta_7 = 0.32(2)$ were tentatively assigned to the so-called Roth-type structure. The latter

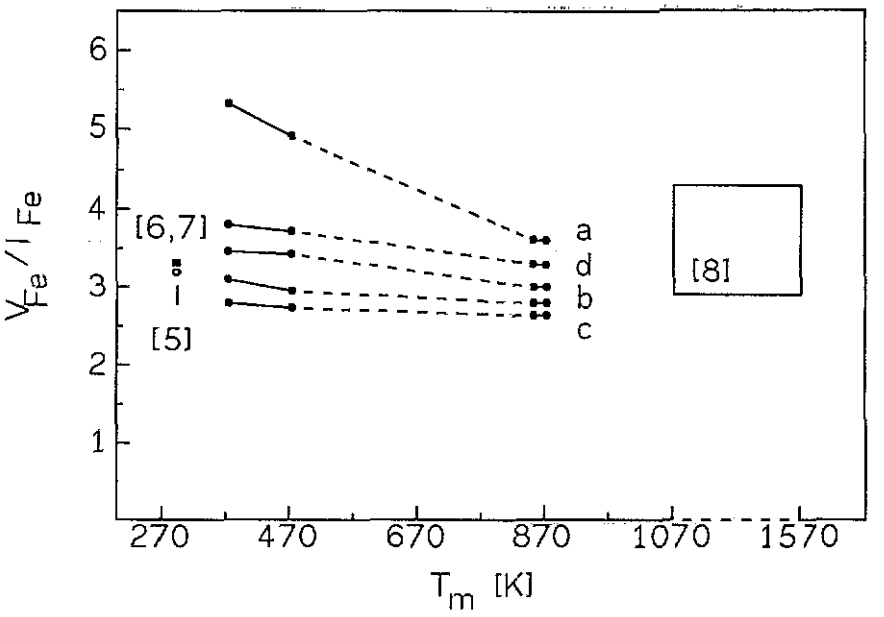

Figure 9. Fe vacancy-to-interstitial ratio V_{Fe}/I_{Fe} in $Fe_{1-x}O$. The full lines and the shaded area represent the value of V_{Fe}/I_{Fe} when f_5 is attributed to: (*a*) the 4:1 complex; (*b*) the 8:3 complex; (*c*) the 10:4 complex; and (*d*) one of the complexes 6:2, 13:4, 16:5 or 10:3. The broken lines connect the full lines through temperature ranges where a sharp PAC signal from Fe_3O_4 has been observed; they do not indicate V/I values. The previous V/I ratios obtained from diffraction measurements are labelled with their references [5–8].

configuration which is visible above 850 K partially seems to develop from the In_s–V_{Fe} configuration. Finally, we discussed the vacancy–interstitial ratios of the proposed defects, in comparison with the values available from x-ray, neutron and electron diffraction and microscopy. At low temperatures, the 4:1 cluster can be eliminated as the dominant component.

Further PAC investigations in cubic metal monoxides appear to be very helpful in our understanding of the defect chemistry in compounds. Studies of TiO, NbO and VO would be particularly profitable because these systems show deviations from stoichiometry on either side of their composition. Such PAC measurements are in progress.

Acknowledgments

The authors are grateful to D Purschke for his help with the ^{111}In implantations and to Mrs H Thomas for the x-ray diffraction analysis. This work has been supported by Deutsche Forschungsgemeinschaft, Projekt Li325/2–1.

References

[1] Seehra M S and Srinivasan G 1984 *J. Phys. C: Solid State Phys.* **17** 883
[2] Hamilton S 1958 *Phys. Rev.* **110**

[3] Chen W K and Peterson N L 1975 *J. Phys. Chem. Solids* **36** 1097
[4] Roth W L 1960 *Acta Crystallogr.* **13** 140
[5] Battle P D and Cheetham A K 1979 *J. Phys. C: Solid State Phys.* **12** 337
[6] Anderson B and Sletnes J O 1977 *Acta Crystallogr.* A **33** 268
[7] Koch F and Cohen J B 1969 *Acta Crystallogr.* B **25** 275
[8] Cheetham A K, Fender B E F and Taylor R I 1971 *J. Phys. C: Solid State Phys.* **4** 2160
[9] Dieckmann R and Schmalzried H 1977 *Berichte der Bunsenges. Phys. Chem.* **81** 344
[10] Catlow C R A and Fender B F F 1975 *J. Phys. C: Solid State Phys.* **8** 3267
[11] Greenwood N N and Howe A T 1972 *J S C Dalton* 110
[12] Bartos A, Bolse W, Lieb K P and Uhrmacher M 1988 *Phys. Lett.* **130A** 177
[13] Bolse W, Uhrmacher M and Lieb K P 1987 *Phys. Rev.* B **36** 1818
[14] Wiarda D, Uhrmacher M, Lieb K P, Wentzel T and Bartos A 1990 *Proc. XXV Zakopane School of Physics* (Singapore: World Scientific) p 340
[15] Kramers H 1952 *Physica* **18** 101
[16] Inglot Z, Wegner D and Lieb K P 1989 *Hyperfine Interact.* **50** 785
[17] Bolse W, Bartos A, Kesten J, Uhrmacher M and Lieb K P 1988 *Proc. XXIII Zakopane School of Physics (Poland, 1988)* (Krakow: Institute of Physics) p 187
[18] Rinneberg H H and Shirley D A 1976 *Phys. Rev.* B **13** 2138
[19] Wegner D, Inglot Z and Lieb K P 1990 *Ber. Bunsensges. Phys. Chem.* **94** 1
[20] Smuts J 1966 *Iron and Steel Instrum.* **204** 237
[21] Shirane G, Cox D E and Ruby S L 1962 *Phys. Rev.* **125** 1158
[22] Hrynkiewicz H U, Kulgawczuk D S, Mazanek E S, Pustowka A M, Tomala K and Wyderko M E 1972 *Phys. Status Solidi* a **9** 611
[23] Johnson D P 1967 *Solid State Commun.* **7** 1785
[24] Greenwood N N and Howe A T 1972 *J S C Dalton* 116
[25] Greenwood N N and Howe A T 1972 *J S C Dalton* 122
[26] Frauenfelder H and Steffen R M 1965 *Alpha, Beta and Gamma Ray Spectroscopy* vol II ed K Siegbahn (Amsterdam: North-Holland) p 997
[27] Hamilton W D (ed) 1975 *The Electromagnetic Interaction in Nuclear Spectroscopy* (Amsterdam: North-Holland)
[28] Rinneberg H H 1979 *Atomic Energy Rev.* **17** 477
[29] Yates M J L 1965 *Alpha, Beta and Gamma Ray Spectroscopy* vol II ed K Siegbahn (Amsterdam: North-Holland) p 1691
[30] Rogers J D and Vasquez A 1975 *Nucl. Instrum. Methods* **130** 539
[31] Uhrmacher M, Pampus K, Bergmeister F J, Purschke D and Lieb K P 1985 *Nucl. Instrum. Methods* B **9** 234
[32] Raether F, Wiarda D, Lieb K P, Chevallier J and Weyer G 1989 *Z. Phys. B. Condensed Matter* **73** 467
[33] James F and Ross M 1977 Program MINUIT, CERN Program Library
[34] Recknagel E 1974 *Hyperfine Interaction Studies by Nuclear Reaction and Decay* ed E Karlson and R Wappling (Sweden: University of Uppsala)
[35] Asai K, Okada T and Sekizawa H 1985 *J. Phys. Soc. Japan* **54** 4325
[36] Kundig W and Hargrowe R S 1969 *Solid State Commun.* **7** 312
[37] Vandenberghe R E and De Grave E 1989 *Mössbauer Spectroscopy Applied to Inorganic Chemistry* vol 3 ed G J Long and F Grandjen (New York: Plenum) p 59
[38] Koch F B and Fine M E 1967 *J. Appl. Phys.* **38** 1470
[39] Wegner D, Inglot Z and Lieb K P 1990 *Hyperfine Interaction* **59** 313
[40] Bartos A and Wenzel T 1991 private communication
[41] Hentschel B 1970 *Z. Naturforsch.* a **25** 1986